

Photochemical Electron Transfer Reactions of Tirapazamine[†]

James S. Poole¹, Christopher M. Hadad¹, Matthew S. Platz^{*1}, Zachary P. Fredin¹, Laura Pickard¹, Elisa Levya Guerrero¹, Margarita Kessler¹, Goutam Chowdhury², Delshanee Kotandeniya² and Kent S. Gates²

¹Department of Chemistry, The Ohio State University, Columbus, OH and

²Department of Chemistry and Biochemistry, University of Missouri, Columbia, MO

Received 22 August 2001; accepted 17 January 2002

ABSTRACT

The absorption and fluorescence spectra of 3-aminobenzo-1,2,4-triazine di-*N*-oxide (tirapazamine) have been recorded and exhibit a dependence on solvent that correlates with the Dimroth E_{T30} parameter. Time-dependent density functional theory calculations reveal that the transition of tirapazamine in the visible region is $\pi \rightarrow \pi^*$ in nature. The fluorescence lifetime is 98 ± 2 ps in water. The fluorescence quantum yield is ~ 0.002 in water. The fluorescence of tirapazamine is efficiently quenched by electron donors via an electron-transfer process. Linear Stern–Volmer fluorescence quenching plots are observed with sodium azide, potassium thiocyanate, guanosine monophosphate and tryptophan (Trp) methyl ester hydrochloride. Guanosine monophosphate, tyrosine (Tyr) methyl ester hydrochloride and Trp methyl ester hydrochloride appear to quench the fluorescence at a rate greater than diffusion control implying that these substrates complex with tirapazamine in its ground state. This complexation was detected by absorption spectroscopy.

INTRODUCTION

Since the late 1980s, a considerable amount of attention has been given to 3-aminobenzo-1,2,4-triazine di-*N*-oxide (tirapazamine; **1**) as a potential antitumor agent, either alone or as part of combination therapies (1). Tirapazamine has been found to be capable of acting selectively in hypoxic environments found in rapidly growing tumors (2,3). One of the proposed mechanisms of action of this compound is shown in Scheme 1: enzymatic electron transfer and subsequent proton transfer to generate the radical **3**, which un-

dergoes β -fission (4) to generate 3-aminobenzo-1,2,4-triazine-*N*-oxide (**4**) and hydroxyl radical, which is well established as a promoter of nucleic acid cleavage (5). The fact that this reaction sequence may be quenched in the presence of oxygen gives rise to the potential *in vivo* selectivity of this agent.

The enzymatically triggered series of reactions can, in principle, be mimicked by light-induced electron-transfer reactions in aqueous solution. The present study was undertaken to investigate that possibility.

MATERIALS AND METHODS

Tirapazamine was synthesized according to the procedure of Fuchs *et al.* (6) All other materials were obtained from commercial sources and used without additional purification. UV–vis spectra were recorded using either a Lambda 6 UV–Visible spectrometer (Perkin Elmer, Norwalk, CT) or a CHEM2000 photodiode array instrument (Ocean Optics, Dunedin, FL). Fluorescence, fluorescence quantum yield (ϕ_f) and fluorescence quenching experiments were carried out using a Spex Fluorolog 1680 double spectrometer (JY Horiba Inc., Edison, NJ). The sample cavity of this instrument could be altered to accommodate an optically transparent quartz dewar for the phosphorescence experiments attempted in vitreous matrices at 77 K.

Fluorescence quenching experiments. A solution of the quencher studied was serially diluted in phosphate buffer (0.025 M, pH 6.9), and an aliquot of tirapazamine solution (in water, final concentrations in buffer solution ranged between 1.0×10^{-5} and 2.0×10^{-4} M tirapazamine) was added. The emission at 555 nm was measured for each sample, and the data obtained subjected to Stern–Volmer analysis (see subsequent section). For each quencher, at least two concentrations of tirapazamine were used to confirm experimentally the expected independence of quenching behavior with **1**.

The fluorescence lifetime, τ_f , was determined by a time-correlated single photon counting (TCSPC) experiment. The system used has been described in detail in previous communications (7).

Theoretical calculations. The UV–vis spectrum of **1** was simulated by time-dependent density functional theory (TD-DFT) (8–11). Geometry optimization and vibrational frequency calculations were performed at the B3LYP/6–31G* level of theory (12–14), using the GAUSSIAN 98 program suite (15). For the tirapazamine anion, the B3LYP/6–31+G* level was used for geometry and vibrational frequency calculations. TD-DFT calculations used the B3LYP/6–31+G** level to calculate the vertical excitation energies for both tirapazamine and its anions. The optimized geometries, energies and vibrational frequencies are available as supplementary material.

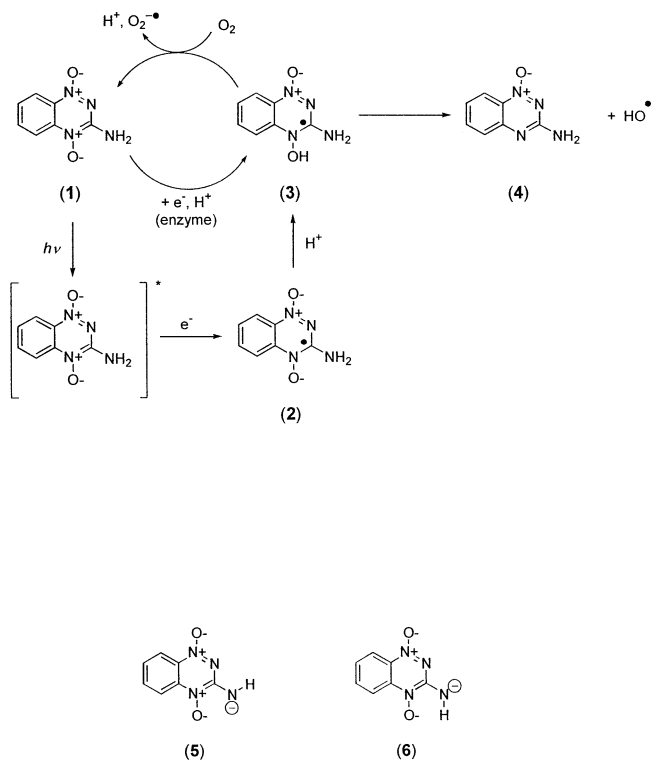
Thermal denaturation (T_m) measurements. The effect of added tirapazamine on the thermal denaturation of DNA duplexes composed of the following sequences was investigated: 5'-(dA)₂₄, 5'-dGTACATCTAACTTGATCTAGTC and 5'-dGTGGTAGATGTC-ATGTC. To prepare the DNA duplexes, equimolar amounts of the oligonucleotide of interest and its complement were dissolved in 20

[†]Posted on the web site on January 28, 2002.

*To whom correspondence should be addressed at: Department of Chemistry, Ohio State University, 100W 18th Avenue, Columbus, OH 43210, USA. Fax: 614-292-5151; e-mail: platz.1@osu.edu

Abbreviations: AMP, adenosine 5' monophosphate; DABCO, 1,4-diazabicyclo[2.2.2]octane; GMP, guanosine monophosphate; 2-MeTHF, 2-methyltetrahydrofuran; TCSPC, time-correlated single photon counting; TD-DFT, time-dependent density functional theory; tirapazamine, 3-aminobenzo-1,2,4-triazine di-*N*-oxide; Trp, tryptophan; Tyr, tyrosine.

© 2002 American Society for Photobiology 0031-8655/02 \$5.00+0.00



Scheme 1.

mM N-2-hydroxyethylpiperazine-N'-2-ethane-sulfonic acid (HEPES), pH 7, to achieve a final concentration of 18–24 μM (base pairs), heated briefly to 90°C and then allowed to hybridize by cooling slowly to room temperature over the course of several hours. The melting temperature of the duplex alone was compared with the melting temperature of the duplex in the presence of tirapazamine (18–24 μM). In the melting experiments, UV-vis spectra were recorded using a Hewlett-Packard 8452A diode array spectrophotometer fitted with a Peltier device. Melting of the DNA duplex was determined by measuring the increase in absorbance at 260 nm while heating the samples at a rate of 1°C in 2 min. The melting temperature was determined from the absorbance data using procedures described previously (16).

Equilibrium dialysis. A solution (200 μL) of tirapazamine (10 μM) and herring sperm DNA (500 μM bp) in HEPES buffer (20 mM, pH 7.0, containing 100 mM NaCl) was placed in a mini-dialysis unit (molecular weight cutoff 3500; Slide-A-Lyzer; Pierce Chemicals Co., Rockford, IL) and dialyzed for 48 h at room temperature with gentle stirring against an identical solution (except that it contained no DNA; 5 mL) of tirapazamine. After 48 h, the concentrations of tirapazamine inside the dialysis unit and outside, in the dialysate, were determined by measuring the absorbance of the drug at 464 nm. Readings were corrected for any background absorbance at this wavelength (by subtracting the absorbance at 464 nm measured in a control experiment in which there was no drug). The binding constant (K_b) can be calculated from these experiments using the equation:

$$K_b = \frac{[\text{ligand} \cdot \text{DNA}]}{[\text{ligand}][\text{DNA}]} \quad (1)$$

where [ligand], [DNA] and [ligand·DNA] are concentrations of free ligand, free DNA and DNA-bound ligand, respectively. The results of seven experiments were averaged, and no evidence for association of tirapazamine with duplex DNA was found.

UV-vis monitoring of tirapazamine titrated with duplex DNA. Absorption spectra were collected using a Hewlett-Packard 8452A diode array spectrophotometer. The effect of duplex DNA on the absorbance spectra of tirapazamine was measured by adding 2–5 μL aliquots of a stock solution of herring sperm DNA (30 mM bp in

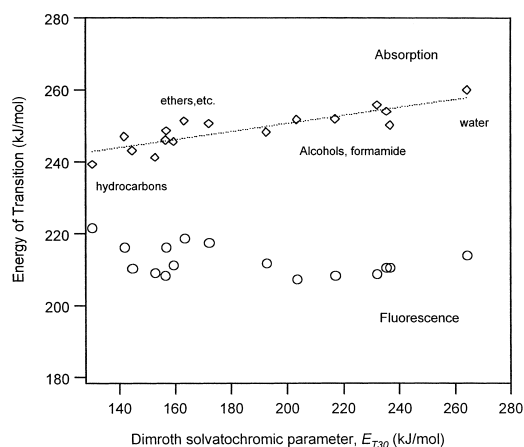


Figure 1. Correlation of the observed absorption and fluorescence maxima for tirapazamine (expressed in kJ mol^{-1}) with the Dimroth solvatochromic parameter (E_{T30}). **1** was only sparingly soluble in cyclohexane, and therefore multiple signal averaging of the resultant dilute solutions was required to identify the absorption and emission maxima.

water) to 3 mL of a solution containing tirapazamine (20 μM) in 50 mM sodium phosphate, pH 7, in a quartz cuvette until a maximum concentration of 1 mM bp DNA was reached. Each addition of DNA was accompanied by addition of an appropriate amount of a concentrated stock of drug in order to keep the ligand concentration constant throughout the course of the experiment. Before recording the spectrum of tirapazamine at each DNA concentration, the spectrophotometer was blanked on an identical solution containing all components except the drug. The resulting spectra were analyzed for changes in tirapazamine's absorbance maximum at 464 nm (changes in the compound's 260 nm absorbance maximum were obscured by the absorbance of DNA at 260 nm). When corrected for the effects of dilution by an appropriate solution of phosphate buffer (equivalent to the concentration of DNA phosphate residues), no changes in the absorbance of the tirapazamine at 464 nm caused by the addition of DNA were found. Identical results were obtained when these experiments were performed in the presence of 100 mM NaCl.

RESULTS

The absorption spectrum of tirapazamine consists of a strong UV band at 266 nm ($\log_{10}\epsilon = 4.56$) in water and a weaker band in the visible at 461 nm ($\log_{10}\epsilon = 3.80$). The spectrum remains relatively unchanged over a pH range of 4–10, but at higher pH values (12 and above), the visible transition is significantly red-shifted to $\lambda_{\text{max}} = 542$ nm ($\log_{10}\epsilon \approx 3.52$). In addition to the foregoing observations, it was found that the visible absorption maximum is strongly dependent on solvent polarity, and a correlation between the absorption maximum and the Dimroth (17,18) solvatochromic parameter (E_{T30}) was established for a range of solvents (Fig. 1). The absorption exhibits a bathochromic shift, consistent with a $\pi \rightarrow \pi^*$ transition (19) in the visible range, similar to that of pyridine-*N*-oxide (20,21). The correlation of $E(\lambda_{\text{max}})$ with E_{T30} is good, but the slope has a relatively small magnitude, suggesting that solvent-solute charge-transfer interactions are unimportant for this species. By contrast, the correlation of the emission energy with E_{T30} is poor. This may be in part because of the fact that the lifetime of solvent reorientation (19) in the cybotactic region (10^{-12} to 10^{-10} s) is comparable to the lifetime of the excited state (see following). Under such conditions, a strong correlation is not expected.

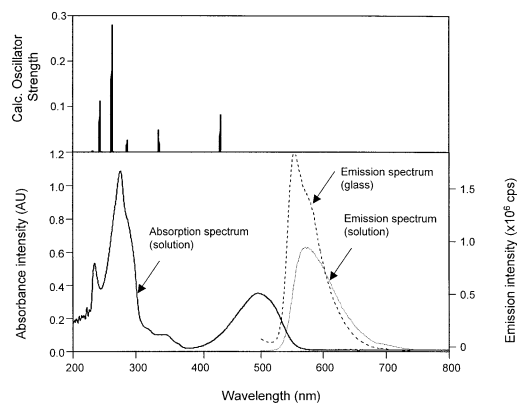


Figure 2. Normalized absorption and emission spectra of **1** in 2-MeTHF. Emission spectra were obtained in both room temperature solution (dotted line) and glass at 77 K (dashed line). The emission spectrum in solution is some 20 times less intense than that in the glass and is not shown to scale. No additional or enhanced features consistent with phosphorescent emission were observed either at room temperature or at 77 K. The UV-vis line spectrum calculated for **1** *in vacuo* by TD DFT calculations is shown in the top section of the figure.

Time-dependent density functional calculations were performed on tirapazamine optimized under C_1 and C_s symmetry constraints at the B3LYP/6-31G* level of theory. Optimization under C_s constraints generated a geometry corresponding to the transition state for inversion of the 3-amino group. However, the energy difference between this transition state and the C_1 minimum (3-amino group being pyramidal) was less than 0.5 kJ mol⁻¹, and the electronic spectra predicted by TD-DFT for both C_1 and C_s geometries remained largely unchanged. The data obtained are available as supplementary material.

TD-DFT calculations at the B3LYP/6-31+G**//B3LYP/6-31G* level of theory indicate that the low-energy transition is a $\pi \rightarrow \pi^*$ transition (predicted by theory to be at 434 nm *in vacuo*). The $n \rightarrow \pi^*$ transitions are predicted to occur at higher energies and with relatively weak oscillator strengths. The simulated *in vacuo* line spectrum is shown relative to the spectrum measured in 2-methyltetrahydrofuran (2-MeTHF) in Fig. 2, and the properties of the calculated spectrum are shown in Table 1.

Similar DFT and TD-DFT calculations were carried out on the anion of tirapazamine formed by loss of a proton from the 4-amino group. Of the two possible isomeric anions **5** and **6**, it was found that anion **6** was the more stable (at the B3LYP/6-31+G* level of theory) by approximately 20 kJ mol⁻¹. Both anions exhibited C_s symmetry. TD-DFT calculations at B3LYP/6-31+G**//B3LYP/6-31G* level for **6** (Table 2) predict a large redshift in the absorbance of the $\pi \rightarrow \pi^*$ band upon deprotonation of **1**, and this qualitative behavior was observed experimentally ($\lambda_{\max} = 542$ nm at pH values above 12).

The fluorescence lifetime, τ_f , of tirapazamine was measured in water, acetonitrile and formamide using time-correlated single photon counting, as described previously. The excitation wavelength used was 320 nm, with a laser pulse width of 4 ps. The emission was measured between 555 and 560 nm. The absorbance of tirapazamine at 320 nm, and hence the emission signal, is low, thus resulting in extended

Table 1. Time-dependent DFT simulation of the electronic spectrum of tirapazamine at the B3LYP/6-31 + G**//B3LYP/6-31G* level of theory*

Symmetry	Orbitals	Weighting coeff.†	Energy (nm)	Energy (eV)	Oscillator strength
A'	46‡ → 47§	0.583	444.7	2.79	0.1033
A''	45 → 47	0.694	353.8	3.50	0.0002
A'	44 → 47	-0.276	333.1	3.72	0.0404
	46 → 48	0.605			
A''	42 → 47	0.685	331.8	3.74	0.0000
A'	43 → 47	0.380	292.7	4.24	0.0231
	44 → 47	0.468			
	46 → 49	0.282			
A'	43 → 47	0.492	268.1	4.62	0.3316
	44 → 47	-0.310			
	46 → 48	-0.226			
A'	41 → 47	0.396	266.2	4.66	0.0186
	46 → 49	0.487			
A''	46 → 50	0.681	251.9	4.92	0.0069
A'	41 → 47	0.499	250.3	5.09	0.1188
	46 → 49	-0.330			
A''	45 → 48	0.701	241.7	5.13	0.0000

No. of states = 10, and only spin-allowed transitions were considered. The planar C_s geometry (B3LYP/6-31G) was used.

†Only coefficients with absolute values >0.2 are included in the table.

‡HOMO.

§LUMO.

Table 2. Time-dependent DFT simulation of the electronic spectrum of tirapazamine anion **6** at the B3LYP/6-31+G**//B3LYP/6-31+G* level of theory*

Symmetry	Orbitals	Weighting coeff.†	Energy (nm)	Energy (eV)	Oscillator strength
A'	46‡ → 47§	0.614	617.1	2.01	0.0532
A''	44 → 47	0.329	382.6	3.24	0.0000
	46 → 48	0.619			
A''	44 → 47	0.611	382.1	3.24	0.0003
	46 → 48	-0.335			
A'	45 → 47	-0.458	367.5	3.37	0.0281
	46 → 49	0.483			
A''	42 → 47	0.502	328.8	3.77	0.0000
	43 → 47	0.472			
A'	45 → 47	0.223	328.3	3.78	0.1252
	46 → 49	0.325			
	46 → 51	0.518			
A''	46 → 50	0.698	323.5	3.83	0.0086
A''	46 → 52	0.665	308.1	4.02	0.0099
A''	42 → 47	0.467	307.6	4.03	0.0001
	43 → 47	0.505			
A'	45 → 47	0.378	301.9	4.11	0.2572
	46 → 49	0.255			
	46 → 51	-0.396			

*No. of states = 10, and only spin-allowed transitions were considered. The planar C_s geometry **6** (B3LYP/6-31 + G*) was used.

†Only coefficients with absolute values > 0.2 are included in the table.

‡HOMO.

§LUMO.

Table 3. Determination of fluorescence quantum yield by comparison with literature standards

Compound	Solvent	λ_{ex} (nm)	Emission range (nm)	$\phi_{f,S}$	Ref.	$\phi_{f,1}$ calc.
Tirapazamine	H ₂ O	470	480–750	—		1.8×10^{-3}
Rhodamine 6G	H ₂ O	470	480–750	0.76*	29	
Tirapazamine	H ₂ O	430	450–750	—		4.1×10^{-4}
Tirapazamine	CHCl ₃ [†]	430	450–750	—		5.9×10^{-4}
Acridine Yellow	EtOH [‡]	430	450–750	0.47*	29	
Tirapazamine	H ₂ O	470	480–750	—		1.4×10^{-3}
Fluorescein	NaOH [§]	470	480–750	0.91	29, 30	

*Determined by photocalorimetry. The value used for Rhodamine 6G corresponds to an average value obtained by measuring the quantum yield with excitation at 488 and 546 nm.

^{†‡}Using the following values for refractive indices: distilled water 1.333, ethanol 1.359 and chloroform 1.446.

[§]0.01 M NaOH. The refractive index of this solvent was assumed to be the same as that of water.

^{||}Average value from both references.

data acquisition times and high background counts. The decay histogram obtained was fitted using convolute-and-compare software (22) to allow for instrument response in the absence of tirapazamine, and best results were obtained using a double exponential fit, presumably because of the high background. Despite this, one fitted exponential in each case had a clearly dominant weighting (>65% for acetonitrile, >80% for water and formamide) and corresponded to the fluorescence decay of tirapazamine. The measured lifetimes obtained for tirapazamine in these media were 98 ± 2 ps in water (four replicates), 110 ± 2 ps in acetonitrile (duplicates) and 209 ± 4 ps (four replicates) in formamide.

The fluorescence quantum yield was determined using the methodology described by Fery-Forgues and Lavabre (23). Solutions of tirapazamine and appropriate dye standards (Table 3) with absorbances of approximately 0.1–0.5 in the range 450–500 nm were diluted 1 in 10 and the fluorescence spectrum obtained was in the range 450–750 nm. The emission peaks were integrated (trapezoidal rule, $\Delta\lambda = 1$ nm), and the fluorescence quantum yield of **1** was determined using the following expression:

$$\phi_1 = \frac{A_s F_1 (n_1)^2}{A_1 F_s (n_s)} \phi_{f,S} \quad (2)$$

where A_s , F_s and n_s were the absorbance at the excitation wavelength, integrated emission and refractive index of the standard solution and $\phi_{f,S}$ the fluorescence quantum yield of the dye standard. It was found that fluorescence is not a particularly efficient process for the excited state: the quantum yield is very low, $\phi_f \leq 0.002$ in both water and chloroform.

Attempts were made to detect the triplet state of tirapazamine but were not successful. No phosphorescence was observed upon excitation (475 nm) of tirapazamine in glassy 2-MeTHF at 77 K. A metastable EPR spectrum was not observed when the spectrum was scanned while exciting tirapazamine in 2-MeTHF at 77 K with unfiltered light from a mercury arc lamp.

The fluorescence quenching of **1** was measured for a number of substrates in various solvents, and the data obtained are summarized in Table 4. A number of substrates exhibited the expected linear Stern–Volmer behavior, and the obtained values of the quenching rate coefficient, k_Q , indicate that the

electron transfer reaction occurs at the diffusion-controlled limit for bimolecular reactions. In contrast, DABCO, Trp methyl ester and, to a lesser extent, hydroquinone exhibit nonlinear Stern–Volmer behavior (Fig. 3), presumably because of the formation of an associative complex between quencher and **1**. We believe that complexation is caused by hydrogen bonding rather than by π donor–acceptor interactions because the quenching of **1** by Trp methyl ester becomes linear and diffusion controlled in formamide, a solvent capable of disrupting hydrogen-bonded complexes.

The simplest model for fluorescence quenching with a quencher capable of forming complexes with the fluorescent species yields the following quadratic Stern–Volmer expression (24):

$$\frac{I_0}{I_{[Q]}} = (1 + K_{comp}[Q])(1 + k_Q\tau_f[Q]) \quad (3)$$

where Q is quencher, and K_{comp} is the equilibrium constant for complexation. Unfortunately, only the Stern–Volmer curve for quenching by hydroquinone could be successfully fitted using the above functional form, yielding $k_Q = (6 \pm 3) \times 10^9 M^{-1} s^{-1}$ and $K_{comp} = 2.0 \pm 0.5 M^{-1}$. The quoted errors are standard deviations from the nonlinear least squares fitting of the data.

Formation of an associative complex may be manifested as a shift or change in absorbance of tirapazamine in the presence of these species, and differential UV–Visible spectra of **1** were obtained in the presence of Trp, Tyr (as methyl ester hydrochlorides) and guanosine monophosphate (GMP; as disodium salt). The results are shown in Fig. 4. Differential spectra were also measured in the presence of NaCl to ensure that any shift observed was not caused simply by a change in ionic strength of the solution. The same qualitative behavior was observed for a shift of the absorbance maximum to lower energy wavelengths. This behavior was not observed in the presence of NaCl, which simply gave a marginally higher absorbance with increasing ionic strength, with no apparent shift. The data obtained support our postulated complex formation and in theory allow the determination of K_{comp} for these substrates. In the event of an absorbance shift in the UV–vis spectrum of **1** in the presence of a large excess of quencher Q, the absorbance at any wave-

Table 4. Rates of reaction for electron transfer between tirapazamine and various substrates determined from Stern-Volmer analysis of fluorescence quenching

Quencher, Q	Solvent*	[Q] (M)	Linear fit		k_q ($M^{-1} s^{-1}$)
			$k_Q \tau_f^\ddagger$ (M^{-1})	$R^{2\ddagger}$	
Calf thymus DNA	W	$(0.03-1.3) \times 10^{-3}\S$		quenching not observed	
AMP	W	0.0-0.25		quenching not observed	
NaN_3	W	0.0-1.45	1.19 ± 0.02	0.990	$(1.23 \pm 0.02) \times 10^{10}$
KSCN	W	0.0-2.35	1.15 ± 0.03	0.990	$(1.19 \pm 0.03) \times 10^{10}$
p-Cresol	A	0.0-1.7	0.67 ± 0.01	0.997	$(6.1 \pm 0.1) \times 10^9$
Hydroquinone#	A	0.0-0.75	3.54 ± 0.09	0.988	$(3.21 \pm 0.09) \times 10^{10}$
Indole	A	0.0-1.4	0.83 ± 0.03	0.982	$(7.5 \pm 0.3) \times 10^9$
Tyrosine**	W	0.0-0.35	4.07 ± 0.03	0.999	$(4.15 \pm 0.03) \times 10^{10}$
GMP††	W	0.0-0.48	4.74 ± 0.10	0.994	$(4.96 \pm 0.11) \times 10^{10}$
	W	0.0-0.50	4.87 ± 0.05	0.998	$(4.97 \pm 0.05) \times 10^{10}$
DABCO	A	0.0-1.8		Nonlinear quenching	
Tryptophan**	W	0.0-0.40		Nonlinear quenching	
	F	0.0-0.5	1.55 ± 0.03	0.991	$(7.42 \pm 0.14) \times 10^9$

*W = aqueous phosphate buffer, 0.025 M, pH 6.9; A = acetonitrile; F = formamide.

†Errors quoted are standard deviations on the line of best fit.

‡Goodness of fit parameter.

§Expressed as mole (base pairs) per liter.

||Adenosine monophosphate disodium salt.

#Hydroquinone Stern-Volmer plot exhibits a small curvature; see text.

**Amino acids used as methyl ester hydrochlorides.

††Guanosine monophosphate, monosodium salt.

length may be expressed in the following terms (a derivation is available as supplementary information):

$$\frac{A_{|Q|}}{A_0} = \frac{\left(1 + \frac{A_\infty}{A_0} K_{comp}[Q]\right)}{(1 + K_{comp}[Q])} \quad (4)$$

where A_∞ is the absorbance of a solution of **1** that is completely bound to Q. In the case where A_∞ can be measured to good approximation, the foregoing expression can be fitted to a single variable, K_{comp} . In the case where A_∞ cannot be well approximated from experimental data, Eq. 4 may be used to fit data using a two-variable, nonlinear least squares fit.

Therefore, we attempted to determine K_{comp} for **1** with Tyr and Trp methyl ester hydrochlorides, GMP and adenosine 5'

monophosphate (AMP) (di- and monosodium salts, respectively). In our particular case, the wavelength shifts (and hence the changes in absorbance, ΔA) are small and are therefore subject to significant experimental uncertainty. Because the curve fitting process is also quite sensitive to small errors in the data, it follows that the most reliable results are obtained using the wavelength with maximum ΔA in these cases around 440 nm, for the relative absorbance curves. The curves obtained for Trp, GMP and AMP are shown in Fig. 5.

Nonlinear least squares fitting of the curves obtained to Eq. 4 yielded the following values for K_{comp} : $6.6 \pm 1.0 M^{-1}$ for Trp methyl ester, $7.4 \pm 1.8 M^{-1}$ for Tyr methyl ester, $4.5 \pm 1.1 M^{-1}$ for GMP, $11.3 \pm 1.6 M^{-1}$ for AMP and $1.7 \pm 0.7 M^{-1}$ for hydroquinone in acetonitrile, within experi-

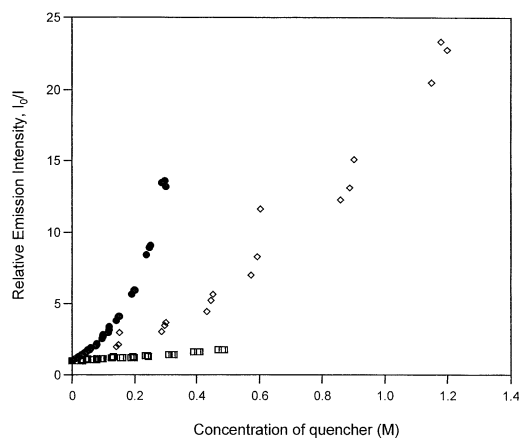


Figure 3. Stern-Volmer plots for fluorescence quenching of **1** with Trp methyl ester hydrochloride in water (solid circles) and formamide (open squares), and DABCO in acetonitrile (open diamonds).

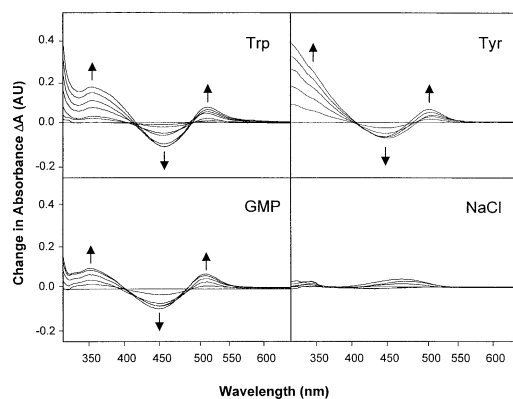


Figure 4. Difference UV-vis spectra of tirapazamine in the presence of Trp methyl ester hydrochloride (Trp, 0.0-0.2 M), Tyr methyl ester hydrochloride (Tyr, 0.0-0.35 M), guanosine monophosphate disodium salt (GMP, 0.0-0.3 M) and NaCl (0.0-3.4 M). Arrows indicate the growth of peaks with increasing concentration of substrate.

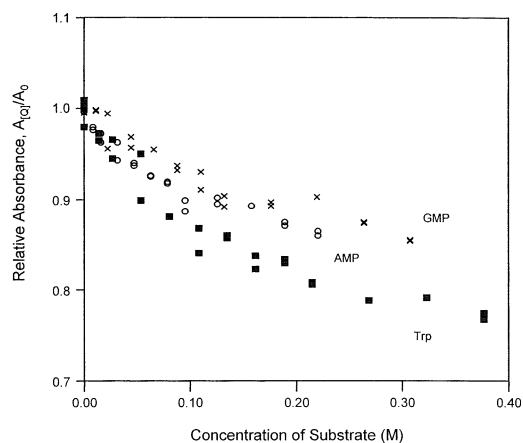


Figure 5. Dependence of relative absorbance of tirapazamine at 440 nm on the concentration of guanosine monophosphate (crosses), adenosine monophosphate (open circles) and Trp methyl ester (solid squares) in aqueous solutions. The curves were subjected to nonlinear least squares fitting to obtain the equilibrium complexation constant, K_{comp} . See text for details.

mental uncertainty of the value obtained from fitting the Stern–Volmer curve (see foregoing discussion). It is worth noting that the data for AMP indicate that **1** forms associative complexes with a number of substrates, but these do not necessarily promote electron transfer between the species.

Attempts to observe enhanced fluorescence quenching by preassociation of tirapazamine with calf thymus DNA, as observed previously for iodoacridine systems, were unsuccessful (25). This observation is consistent with the fact that three different types of experiments reveal no detectable noncovalent association of tirapazamine with duplex DNA. First, we find that tirapazamine does not alter the melting temperature of several different DNA duplexes that vary in GC/AT content. Typically, DNA-binding ligands induce an increase in duplex melting temperatures, T_m (26). However, a significant shift in T_m is expected only if the binding constant K_b of **1** to DNA duplex is significant. UV–vis and dialysis experiments are better suited for detection of moderate binding ($K_b \geq 10^2 M^{-1}$). However, addition of DNA to a solution of tirapazamine does not result in detectable changes in the UV–vis spectrum of the drug. Association of organic compounds with DNA commonly results in significant changes in the UV–vis spectrum of the ligand (27). Finally, equilibrium dialysis experiments show no measurable association of tirapazamine with double-stranded DNA.

The lack of complexation of **1** with double-stranded DNA is consistent with the fact that **1** forms hydrogen-bonded complexes with AMP, GMP and other suitable substrates. Such hydrogen bonding sites on G and A are not readily available in double-stranded DNA, but our results indicate that enhanced fluorescence quenching and electron transfer may be available to **1** with single-stranded DNA.

DISCUSSION

Tirapazamine absorbs in the visible region and more strongly in the ultraviolet region of the spectrum. The visible band is a $\pi \rightarrow \pi^*$ transition centered largely around 460–500 nm. Tirapazamine fluorescence shows a weaker dependence on

Table 5. Single-electron oxidation–reduction potentials of tirapazamine and selected molecules of biological interest in pH 7 solution

Compound	E(pH 7) (V)	Ref.
One-electron oxidation		
Tryptophan	1.01	31, 32
Tyrosine	0.94	31, 32
Guanosine	1.29	31, 32
Adenosine	1.42	33
One-electron reduction		
Tirapazamine	−0.45	34

solvent polarity than does absorption. The fluorescence lifetime is 98 ps in water. The major deactivation pathways of the excited singlet state are fluorescence and internal conversion. A number of physical methods (matrix phosphorescence, EPR) failed to provide evidence of the formation of triplet tirapazamine.

The fluorescence of tirapazamine is quenched by Tyr and Trp methyl esters, as well as GMP, at a rate slightly greater than a diffusion-controlled rate in aqueous solution. This implies that Trp, Tyr and GMP form associative, hydrogen-bonded complexes with **1** in its ground state. The fluorescence is also quenched by sodium azide and sodium iodide, but is not quenched by AMP at concentrations between 0.0 and 0.25 M. The data indicate that the singlet excited state of tirapazamine is quenched by electron transfer from suitable donors. We have performed a first-approximation estimation for the energetics of electron-transfer with biologically relevant molecules using the single electron oxidation–reduction potentials shown in Table 5. In each case, the potentials are determined or calculated in a pH 7 solution. If we assume that the $S_{0,0} \rightarrow S_{1,0}$ electronic transition for tirapazamine in water is approximately 510–520 nm (2.4 eV), we find that to a first approximation Trp, Tyr, guanosine and adenosine all satisfy at least the energetic requirement for electron transfer.

Our results indicate that the previously reported tirapazamine photosensitized DNA cleavage (28) proceeds through the singlet state of the sensitizer and is initiated by electron transfer from a guanine residue. The rate of electron transfer is diffusion limited, as **1** does not form associative complexes with DNA. DNA cleavage is suppressed by the presence of oxygen. Oxygen must scavenge radical or radical ion intermediates, which cleave DNA *after* the initial electron transfer process. Attempts to detect these species are in progress. Our data also indicate that photolysis of tirapazamine in the presence of protein will oxidize Tyr and Trp residues.

CONCLUSIONS

The photophysics of the antitumor drug tirapazamine have been investigated by spectroscopic and computational methods. Tirapazamine has a band in the visible region assigned as a $\pi \rightarrow \pi^*$ transition on the basis of TD-DFT calculations. This transition is sensitive to solvent polarity. The solvent effect correlates with the Dimroth E_{T30} scale. The fluorescence lifetime of tirapazamine in water is 98 ps, and the fluorescence quantum yield is ≤ 0.002 . The triplet state was not detected by either matrix or phosphorescence spectroscopy.

copy. The fluorescence of tirapazamine is efficiently quenched by electron donors. Photolysis of tirapazamine in the presence of nucleic acid and protein will lead to oxidation of guanine and Trp residues, respectively. It is concluded that photolysis of tirapazamine in the presence of electron donors may mimic the first step of the activation of tirapazamine *in vivo*, thus providing a potentially useful new method for studying the properties of tirapazamine under well-defined conditions.

Acknowledgements—Support of this work by the NSF-Environmental Molecular Science Institute at The Ohio State University (NSF CHE-0089147 to M.S.P. and C.M.H.) and the American Cancer Society (RPG 00-028-01 to K.S.G.) is gratefully acknowledged, as are the computational resources made available from the Ohio Supercomputer Center. The authors would also like to thank Terry Gustafson and Frank DeLucia Jr. at OSU for performing the TCSPC experiments.

REFERENCES

- Brown, J. M. (1999) The hypoxic cell: a target for selective cancer therapy—eighteenth Bruce F. Cain memorial award lecture. *Cancer Res.* **59**, 5863–5870.
- Costa, A. K., M. A. Baker, J. M. Brown and J. R. Trudell (1989) *In vitro* hepatotoxicity of SR 4233 (3-amino-1,2,4-benzotriazine-1,4-dioxide), a hypoxic cytotoxin and potential antitumor agent. *Cancer Res.* **49**, 925–929.
- Brown, J. M. (1993) SR 4233(tirapazamine): a new anticancer drug exploiting hypoxia in solid tumors. *Br. J. Cancer* **67**, 1163–1170.
- Daniels, J. S. and K. S. Gates (1996) DNA cleavage by the antitumor agent 3-amino-1,2,4-benzotriazine 1,4-dioxide (SR4233): evidence for involvement of hydroxyl radical. *J. Am. Chem. Soc.* **118**, 3380–3385.
- Von Sonntag, C., U. Hagen, A. Schoen-Bopp and D. Schulte-Frohlinde (1981) Radiation-induced strand breaks in DNA: chemical and enzymic analysis of end groups and mechanistic aspects. *Adv. Radiat. Biol.* **9**, 109–142.
- Fuchs, T., G. Chowdhury, C. L. Barnes and K. S. Gates (2001) 3-Amino-1,2,4-benzotriazine 4-oxide: characterization of a new metabolite arising from bioreductive processing of the antitumor agent 3-amino-1,2,4-benzotriazine 1,4-dioxide (tirapazamine). *J. Org. Chem.* **66**, 107–114.
- Buterbaugh, J. S., J. P. Toscano, W. L. Weaver, J. R. Gord, C. M. Hadad, T. L. Gustafson and M. S. Platz (1997) Fluorescence lifetime measurements and spectral analysis of adamantyldiazirine. *J. Am. Chem. Soc.* **119**, 3580–3591.
- Bauernschmitt, R. and R. Ahlrichs (1996) Treatment of electronic excitations within the adiabatic approximation of time dependent density functional theory. *Chem. Phys. Lett.* **256**, 454–464.
- Stratmann, E. R., G. E. Scuseria and M. J. Frisch (1998) An efficient implementation of time-dependent density-functional theory for the calculation of excitation energies of large molecules. *J. Chem. Phys.* **109**, 8218–8224.
- TD-DFT has been used successfully to simulate electronic spectra (vertical transitions) of organic molecules. For example, see Wiberg, K. B., R. E. Stratmann and M. J. Frisch (1998) A time-dependent density functional theory study of the electronically excited states of formaldehyde, acetaldehyde and acetone. *Chem. Phys. Lett.* **297**, 60–64.
- van Gisbergen, S. J. A., A. Rosa, G. Ricciardi and E. J. Baerends (1999) Time-dependent density functional calculations on the electronic absorption spectrum of free base porphyrin. *J. Chem. Phys.* **111**, 2499–2506.
- Becke, A. D. (1988) Density-functional exchange-energy approximation with correct asymptotic behavior. *Phys. Rev. A* **38**, 3098–3100.
- Becke, A. D. (1993) Density-functional thermochemistry. III. The role of exact exchange. *J. Chem. Phys.* **98**, 5648–5652.
- Lee, C., W. Yang and R. G. Parr (1988) Development of the Colle-Salvetti correlation-energy formula into a functional of the electron density. *Phys. Rev. B* **37**, 785–789.
- Frisch, M. J., G. W. Trucks, H. B. Schlegel, G. E. Scuseria, M. A. Robb, J. R. Cheeseman, V. G. Zakrzewski, J. A. Montgomery, Jr., R. E. Stratmann, J. C. Burant, S. Dapprich, J. M. Millam, A. D. Daniels, K. N. Kudin, M. C. Strain, O. Farkas, J. Tomasi, V. Barone, M. Cossi, R. Cammi, B. Mennucci, C. Pomelli, C. Adamo, S. Clifford, J. Ochterski, G. A. Petersson, P. Y. Ayala, Q. Cui, K. Morokuma, D. K. Malick, A. D. Rabuck, K. Raghavachari, J. B. Foresman, J. Cioslowski, J. V. Ortiz, B. B. Stefanov, G. Liu, A. Liashenko, P. Piskorz, I. Komaromi, R. Gomperts, R. L. Martin, D. J. Fox, T. Keith, M. A. Al-Laham, C. Y. Peng, A. Nanayakkara, C. Gonzalez, M. Challacombe, P. M. W. Gill, B. Johnson, W. Chen, M. W. Wong, J. L. Andres, C. Gonzalez, M. Head-Gordon, E. S. Replogle and J. A. Pople (1998) *Gaussian 98, Revision A.6*. Gaussian, Inc. Pittsburgh, PA.
- McDowell, J. A. and D. H. Turner (1996) Investigation of the structural basis of thermodynamic stabilities of tandem GU mismatches: solution structure of (rGAGGUCUC)₂ by two-dimensional NMR and simulated annealing. *Biochemistry* **35**, 14077–14089.
- Dimroth, K. and C. Reichardt (1969) Erweiterung der lösungsmittelpolaritätsskala durch verwendung alkyl-substituierter pyridinium-*N*-phenol betaine. *Liebigs Ann. Chem.* **727**, 93–99.
- Reichardt, C. (1979) *Solvent Effects in Organic Chemistry*, pp. 225–262. Verlag Chemie, Weinheim.
- Reichardt, C. (1979) *Solvent Effects in Organic Chemistry*, pp. 189–205. Verlag Chemie, Weinheim.
- Bist, H. D., J. S. Parihar and J. C. D. Brand (1976) The 341 nm band system of pyridine-*N*-oxide. Analysis of the in-plane vibrational structure. *J. Mol. Spectrosc.* **59**, 435–441.
- Brand, J. C. D. and K. T. Tang (1971) Rotational analysis of the 342 nm band of pyridine-*N*-oxide. *J. Mol. Spectrosc.* **39**, 171–174.
- Demas, J. N. and S. Snyder (1989) *Single Photon Counting Software*.
- Fery-Forgues, S. and D. Lavabre (1999) Are fluorescence quantum yields so tricky to measure? A demonstration using familiar stationary products. *J. Chem. Ed.* **76**, 1260–1264.
- Birks, J. B. (1970) *Photophysics of Aromatic Molecules*, pp. 443–448. Wiley-Interscience, London.
- Chen, T., E. Voelk, M. S. Platz and R. P. Goodrich (1996) Photochemical and photophysical studies of 3-amino-6-iodoacridine and the inactivation of λ phage. *Photochem. Photobiol.* **64**, 622–631.
- Wilson, W. D., F. A. Tanius, M. Fernandez-Saiz and C. T. Rigel (1997) *Evaluation of Drug-Nucleic Acid Interactions by Thermal Melting Curves, Drug-DNA Interaction Protocols* Vol. 90, (Edited by K. R. Fox), pp. 219–239. Humana, Totowa, NJ.
- Jenkins, T. (1997) *Optical Absorbance and Fluorescence Techniques for Measuring DNA-Drug Interactions*; Vol. 90 (Edited by K. R. Fox), pp. 195–218. Humana Press, Totowa, NJ.
- Daniels, J. S., T. Chatterji, L. R. MacGillivray and K. S. Gates (1998) Photochemical DNA cleavage by the antitumor agent 3-amino-1,2,4-benzotriazine 1,4-dioxide (tirapazamine, WIN 59075, SR4233). *J. Org. Chem.* **63**, 10027–10030.
- Olmstead, J. III (1979) Calorimetric determinations of absolute fluorescence quantum yields. *J. Phys. Chem.* **83**, 2581–2584.
- Martin, M. M. (1975) Hydrogen bond effects on radiationless electronic transitions in xanthene dyes. *Chem. Phys. Lett.* **35**, 105–111.
- DeFelippis, M. R.; C. P. Murthy, F. Broitman, D. Weinraub, M. Farraggi and M. H. Klapper (1991) Electrochemical properties of tyrosine phenoxo and tryptophan indolyl radicals in peptides and amino acid analogs. *J. Phys. Chem.* **95**, 3416–3419.
- Jovanovic, S. V.; S. Steenken and M. G. Simic (1991) Kinetics and energetics of one-electron-transfer reactions involving tryptophan neutral and cation radicals. *J. Phys. Chem.* **95**, 684–687.
- Steenken, S. and S. V. Jovanovic (1997) How easily oxidizable is DNA? One-electron reduction potentials of adenosine and guanosine radicals in aqueous solution. *J. Am. Chem. Soc.* **119**, 617–618.
- Priyadarsini, K. I., M. Tracy and P. Wardman (1996) The one-electron reduction potential of 3-amino-1,2,4-benzotriazine 1,4-dioxide (tirapazamine): a hypoxia-selective bioreductive drug. *Free Rad. Res.* **25**, 393–399.